Cellular and Molecular Biology
E-ISSN : 1165-158X / P-ISSN : 0145-5680
www.cellmolbiol.org

Ferroptosis-associated lncRNA prognostic signature predicts prognosis and immune response in laryngeal squamous carcinoma

Yuan Dong[1,2], Kai Zhao[2], Qibing Qiu[1], Shikang Zheng[2], Xiaoran Zhang[3], Jinjing Liu[4], Haiming Xu[4], Xiazhi Pan[3], Mingbo Liu[1,2*]

[1] The Second School of Clinical Medicine, Southern Medical University, Guangzhou, China
[2] Department of Otolaryngology Head and Neck Surgery, Hainan Hospital of Chinese PLA General Hospital, Sanya, China
[3] School of Clinical Medicine, Weifang Medical University, Weifang, China.
[4] Medical School of Chinese PLA, Beijing, China

ARTICLE INFO

Original paper

Article history:
Received: June 25, 2023
Accepted: September 24, 2023
Published: November 30, 2023

Keywords:

lncRNA; prognostic; immune response; laryngeal squamous carcinoma

ABSTRACT

In order to construct a prognostic model of ferroptosis-related lncRNA associated with laryngeal carcinoma and to investigate its prognostic value, RNA sequencing, genomic mutation, and clinical data of laryngeal squamous carcinoma patients were collected from the TCGA database. Patients were randomly divided into train and test groups. Cox regression analysis and lasso regression analysis were performed on the data of patients in the training group, and their independent prognostic effect was validated in the test group and the whole cohort. Data from 123 laryngeal squamous carcinoma patients in the TCGA database were collected. According to previous literature, 484 ferroptosis-related genes were collected, and 912 ferroptosis-related lncRNAs were obtained by co-expression. Cox models suggested six lncRNAs involved in ferroptosis (AC083862.2, CYTOR, AC114296.1, LINC02768, GATA2-AS1, CTB-178M22.2). Patients were divided into high-risk and low-risk groups based on median risk scores. Kapkan-Meier survival curve results showed a statistical difference in survival between the high- and low-risk groups. Receiver operating characteristic curves and principal component analysis demonstrated the high accuracy of the model. Univariate and multifactorial Cox regression analyses and column plots demonstrated risk scores as independent prognostic factors. The distribution of prognostic marker risk scores was correlated with clinical staging. Immune infiltration studies suggested the model was associated with immune checkpoints and multiple immune functions. GATA2-AS1 was able to promote cell proliferation, cell migration, and cell invasion. This study identified six lncRNAs associated with ferroptosis in laryngeal squamous carcinoma as prognostic predictors, which may be promising biomarkers involved in the treatment of laryngeal squamous carcinoma.

Doi: http://dx.doi.org/10.14715/cmb/2023.69.12.36

Introduction

Laryngeal carcinoma is the second most common malignancy of the upper respiratory tract after lung cancer, accounting for approximately 20% of head and neck tumors (1). Laryngeal carcinoma is commonly seen in middle-aged and elderly men, and risk factors include smoking, alcohol, and HPV infection (2). With the increasing incidence of laryngeal carcinoma in recent years, most patients have progressed to advanced stages when diagnosed. By identifying reliable biomarkers, we can predict patients' therapeutic response and prognosis, which has important clinical implications for the formulation of effective treatment strategies for patients.

Regulated cell death (RCD) is a general term for various forms of cell death, a crucial factor affecting cell fate (3). Ferroptosis has been described as a mode of cell death that is dependent on iron and reactive oxygen species (ROS). From a biochemical point of view, ferroptosis is characterized by generating lethal levels of iron-dependent peroxidation reactions (4,5). Like other regulated modes of cell death, ferroptosis is a genetically regulated cell death. Ferroptosis is also accompanied by altered morphological and biochemical characteristics and is highly associated with multiple intracellular metabolic pathways. Metabolic pathways such as iron metabolism, lipid metabolism, and amino acid metabolism directly influence the development of ferroptosis and the susceptibility of cells to ferroptosis.

Long non-coding RNA (lncRNA) is a single-stranded RNA with a unit length of more than 200 nucleotides, most of which cannot encode proteins (6). lncRNAs can participate in various biological processes and play critical roles in them, such as chromosome modification, transcriptional activation, and interference (7). Previous studies have shown that abnormal lncRNA expression can be used as one of the predictors of poor prognosis in many cancers (8-10). Studies on the relationship between ferroptosis-related lncRNAs and the prognosis of laryngeal carcinoma are still relatively vacant. Therefore, exploring ferroptosis-related lncRNA prognostic markers associated with laryngeal carcinoma prognosis can contribute to the diagnosis, treatment, and prevention strategies for laryngeal carcinoma. In this paper, we construct a ferroptosis-related lncRNA prognostic model and identify several lncRNA

* Corresponding author. Email: mingbo666@vip.163.com

markers that provide new clinical ideas to find potential therapeutic targets for laryngeal carcinoma.

Materials and Methods

Data Acquisition

Access the TCGA website (https://portal.gdc.cancer.gov/) and select clinical data on laryngeal carcinoma in HNSC. RNA-Seq data and clinical features of 112 tumor samples and 11 normal samples were obtained, including tumor somatic mutation data, survival time, survival status, age, gender, tumor grade, tumor stage, and tumor TNM classification. Annotation information of lncRNA was obtained from the GENCODE website (https://www.gencodegenes.org/) and processed accordingly.

Identification of ferroptosis-related genes

Ferroptosis-related genes were obtained from a database website (http://www.zhounan.org/ferrdb/current/) (11). A list of 'driver', 'marker' and 'suppressor' genes for ferroptosis was downloaded and collated, resulting in 484 ferroptosis-related genes. Spearman's correlation coefficients were calculated based on the expression profiles of ferroptosis-related genes and lncRNAs, which were screened with the condition of |Cor>0.4|, P<0.001.

Analysis of variances

The lncRNA expression matrix between the selected tumor samples and normal samples was filtered by the "limma" package in R. The criteria for screening the expression matrix of differential lncRNAs were: |log2(fold change)| > 1 and FDR < 0.05.

Construction of Co-expression Network

To demonstrate the correlation between ferroptosis-related lncRNAs and ferroptosis denes, we constructed a co-expression network of lncRNAs and ferroptosis genes by using Cytoscape software(http://www.cytoscape.org/). The Sankey diagram was constructed by the Sangerbox database(http://vip.sangerbox.com/home.html).

Construction of the Survival Analysis Model based on Ferroptosis-Related lncRNA

Cox univariate analysis was performed using the “survival” package in R to identify the cross molecules between ferroptosis-related genes and differentially expressed lncRNAs, determining the potential ferroptosis-related lncRNAs associated with prognosis (P<0.05). Cox regression analysis was conducted on the 111 cases collected to establish the final prognostic model. LASSO-Cox regression analysis was performed using the “glmnet” package in R, with 10-fold cross-validation to select the optimal penalty (λ) and minimum criteria. Subsequently, stepwise Cox regression analysis was performed. The final ferroptosis-related prognostic risk score formula for each patient was as follows: Risk score =, where Coefi represents the coefficient and xi represents the normalized count of ferroptosis-related lncRNAs. Based on the median risk score, 111 patients were divided into high-risk and low-risk groups. The overall survival (OS) was compared between the high and low-risk groups using the “surminer” package in R and the log-rank test. Receiver operating characteristic curves (ROCs) were generated using the ‘timeROC’ package in R to assess the accuracy of the prediction model.

Risk Model Validation

In order to assess the accuracy and diagnostic value of the ferroptosis-related lncRNA prognostic model, the receiver operating characteristic (ROC) curve and the area under the curve (AUC) were calculated using the survival ROC and time ROC curve packages in R. The risk model was validated using principal component analysis (PCA), and the results were visualized using the 'scatterplot3D' package in R. Progression-free survival (PFS) was analyzed using the 'survivor' and 'survminer' packages in R. The accuracy of the risk model was predicted by constructing C-index curves using R packages such as "rms," "dplyr," "survival," and "pec."

Construction of Calibration curves

Univariate and multivariate Cox regression analyses were performed to investigate the risk model and its independent prognostic effects. Based on the univariate and multivariate Cox regression results, we developed calibration curves using the R package 'rms', 'regplot', and 'survivor'.The accuracy of the line plots was evaluated using calibration curves.

Functional Enrichment Analysis

The differential expression genes between the high-risk and low-risk groups were identified using the R package "edgeR," with the criteria of |log2(fold change)| > 1 and FDR < 0.05. The functional enrichment analysis was performed using the R package "clusterProfiler," which utilizes gene ontology (GO) and Kyoto Encyclopedia of Genes and Genomes (KEGG) databases for functional annotation. The statistical significance was determined by adjusted P-value < 0.05.

Immune Cell Infiltration and Immune Checkpoint Evaluation

The infiltration of immune cells was determined using TIMER2.0 (http://timer.cistrome.org/), which provides data on immune cell infiltration (12). This website contains six new algorithms, including CIBERSORT, MCP-counter, quanTIseq, EPIC, xCell, and TIMER. 13 immune-related pathway activities were determined by single-sample gene enrichment analysis (ssGSEA) (13). Potential immune checkpoint genes were obtained from relevant literature to predict immune checkpoints with significance in high and low-risk groups (14).

Drug Sensitivity Prediction

The data were analyzed in "pRRophetic" package to predict the IC50 of a chemotherapeutic drug, which indicated the effectiveness of the substance in inhibiting a specific biological or biochemical process.

Cell Culture

Human laryngeal squamous carcinoma cell lines (TU686 and AMC-HN-8) were purchased from Qingqi (Shanghai, China) Biotechnology Development Co. They were cultured at 37°C, 95% humidity, and 5% CO_2 cell culture incubator using DMEM and 10% fetal bovine serum (Bioexplorer, South America).

RNA Extraction and Quantitative Real-Time Polymerase Chain Reaction (qRT-PCR)

RNA was extracted from the cells using the Total RNA Extreme Extraction Kit (Feige, China) according to the standard protocol. cDNA synthesis was then performed using the cDNA Synthesis Kit. Gene expression was quantified using SYBR Green Master Mix , and gene expression levels were calculated using the 2-DDCt method, using GAPDH as a standard internal reference. All primers used for qRT-PCR were synthesized by Reebok Biotechnology (Guangzhou, China).

CCK-8 Assay

Cells were seeded at 1 x 10^4 cells/well in 96-well plates and were treated with CCK8 assay reagent every 24 hours. Cell proliferation was detected at 450 nm using the CCK-8 assay kit (GLPBIO, USA). After all, assays were completed, the experimental results were statistically analyzed to calculate whether there was any statistical difference between the growth rate of the experimental and control groups and to plot the growth curve.

Clonogenic Assay

The cultured cells were centrifuged to make a cell suspension of 1×10^4 cells/ml, inoculated in 6-well plates at 100 µl per well, and supplemented with complete double antibody-free medium to 2 ml. The medium was changed every 48 hours for a total of 14 days. On the 14th day, the medium was aspirated and washed twice with phosphate-buffered saline (PBS), fixed with 1 ml of fixative for 30 min, rinsed with PBS, and stained with 1 ml of Richter-Gimza staining solution for 30 min. Subsequently, cells were washed with PBS until the background was clean, air-dried, and photographed using a camera.

Wound Healing Assay

Cells were seeded at a density of 5×10^4 cells/well in a 12-well plate. After the cells had adhered and formed a monolayer, a 1000 µ pipette tip was used for the scratching experiment, and one pipette tip was changed for each, replicated well, and the whole operation was performed under a sterile environment using an alcohol lamp. Cells were observed every 6 hours, and the images of the scratch were photographed at 0, 24, and 48 hours and statistically analyzed.

Transwell Assay

Transwell chambers (Corning-Costar, 3422, 354480) were used to assess cell migration and invasion. Cells were inoculated in transwell chambers at a density of 1×10^5/well after 24 h of starvation culture. After 48 hours of incubation, the cells were fixed with methanol and stained with crystal violet. The cells that migrated or invaded through the membrane were observed and photographed under a microscope, and the number of cells that crossed the membrane was quantified.

Statistical analysis

All statistical analyses were performed using the R programming language (version 4.0.3) in R Studio. RNA-seq transcriptome data were downloaded from the TCGA database. The "limma" package in R was used for differential expression analysis. Pearson correlation test was used to analyze the correlation between ferroptosis-related genes and lncRNAs. The "limma" package was used to identify differentially expressed lncRNAs as prognostic markers for ferroptosis. The Cox proportional hazards regression model was used to calculate hazard ratios for univariate and multivariate analyses, and the "Cluster Profiler" package was used to analyze GO and KEGG pathways.

Results

Identification of differentially expressed ferroptosis-related lncRNAs in patients with laryngeal squamous carcinoma

After data downloading and collation, we obtained transcript information from the TCGA database for 111 patients, including 16,876 lncRNAs and 19,938 mRNAs. To identify the set of genes involved in ferroptosis, we obtained ferroptosis-related genes from the Ferrdb database (http://www.zhounan.org/ferrdb/) and we finally got 484 genes(driver, marker, and suppressor). Subsequently, we selected ferroptosis-related lncRNAs based on a correlation coefficient>0.4 and P-value <0.001, resulting in a total of 2,066 ferroptosis-related lncRNAs. Subsequently, we selected ferroptosis-related lncRNAs based on a correlation coefficient >0.4 and P-value <0.001, resulting in a total of 2,066 ferroptosis-related lncRNAs. Using the criteria of log2|fold change| >1 and FDR <0.05, we performed differential expression analysis of ferroptosis-related lncRNAs between normal and tumor tissues, identifying 912 significantly differentially expressed lncRNAs, as shown in Figure 1A, which depicts the volcano plot.

Construction and validation of a prognostic model associated with ferroptosis-related lncRNAs and prognosis

To validate the prognostic potential of ferroptosis-related lncRNAs for patients, we evaluated the prognostic potential of ferroptosis-related lncRNAs by Cox univariate regression analysis based on OS of laryngeal squamous carcinoma patients in the TCGA database. Finally, we obtained 28 ferroptosis-related lncRNAs with prognostic re-

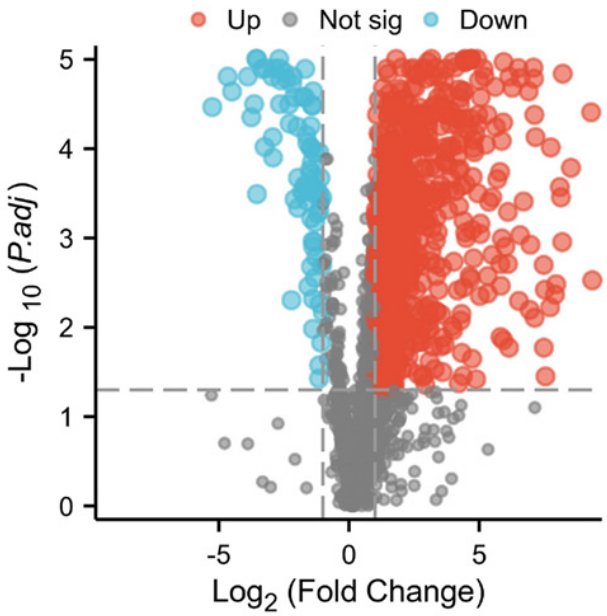

Figure 1. Identification of Differentially Expressed Ferroptosis-Related lncRNAs in Laryngeal Squamous Cell Carcinoma Patients.

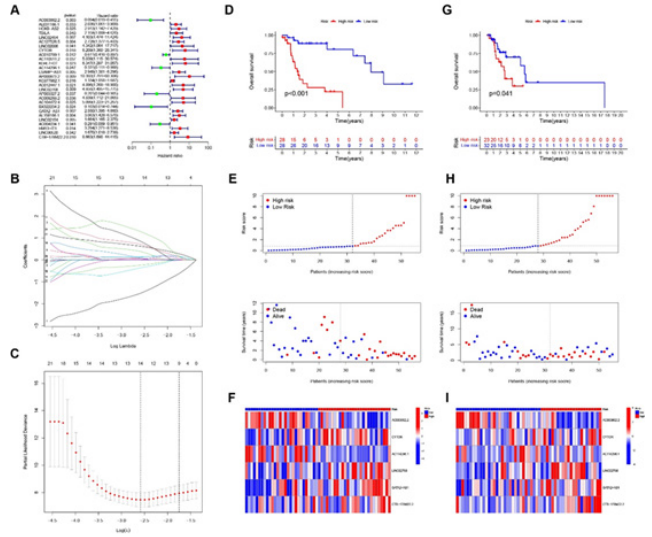

Figure 2. Construction and Validation of the Ferroptosis-Related lncRNA Prognostic Model. (A) Identification of 28 Ferroptosis-Related lncRNAs through Univariate Cox Regression. (B) Lasso coefficient profile of Ferroptosis-Related lncRNAs, each line represents a different lncRNA. (C) Lasso curve of Ferroptosis-Related lncRNAs. (D)-(F) Survival status, risk score, and heatmap of the experimental group. (G)-(I) Survival status, risk score, and heatmap of the validation group.

levance, as shown in Figure 2A and Table 1. Based on the above lncRNAs for lasso regression analysis, 14 ferroptosis-associated lncRNAs were still significant, as shown in Figure 2B-C. We performed multivariate Cox regression, and finally, we obtained six ferroptosis-associated lncRNAs as independent predictors for patients with laryngeal squamous carcinoma. The risk score equation of the prognostic model was constructed as follows: risk score = (-2.87587345360181*AC083862.2)+ (2.22125266265339*CYTOR) + (-1.20694482844275*AC114296.1) + (1.13879131997907*LINC02768) + (1.08543317155557*GATA2-AS1) + (3.32321562463419*CTB-178M22.2).

According to the median risk score, we divided 111 patients into the training group and Test group for analysis, including 56 patients in the training group and 55 patients in the test group, and the general clinical data of the two groups are shown in Table 2. KM survival curve was used to analyze the OS of patients in both groups. The patients in the training group were divided into high and low-risk groups for survival analysis, and the KM survival curve was used to analyze the OS of patients in both groups. The OS of patients in the high-risk group was worse than that in the low-risk group, and the results are shown in Figure 2D. The distribution of risk scores and patient survival in the training group are shown in Figure 2E. The six lncRNAs involved in the high and low-risk groups in the training group Expression levels of the high and low-risk groups in the training group are shown in Figure 2F. The above results show that as the risk score increases, the survival time of patients shortens, and the number of deaths increases. The results obtained in the Test group are similar to the findings in the training group, as shown in Figure 2G-I. The trend of the validation of the results for the whole cohort is the same as the trend of the findings in the two subgroups, as shown in Figure 3A-C. PCA (principal component analysis) shows the degree of differentiation between the high- and low-risk groups. As seen in Figure 3D-G, the patients were effectively divided into two cohorts in the risk model based on iron death-related lncRNA (Figure 3D-G).

Ferroptosis-related lncRNA prognostic markers have independence in predicting the overall survival rate

To explore the independence of the constructed risk model in overall survival, we performed one-way and multiway Cox regression analyses. In the univariate regression analysis, gender and risk score were significant influences, as shown in Figure 4A. In the multifactorial Cox regression analysis, they still provided valid prognostic values ($P < 0.05$) (Figure 4B). Figure 4C shows significant differences in PFS between the high and low-risk groups. The ROC curves indicate the accuracy and diagnostic value of ferroptosis-related lncRNA on OS impact with AUCs of 0.787 at one year,0.820 at two years, and 0.858 at three years (Figure 4D). Figure 4E shows the ROC curves for other clinical traits and risk models, and Figure 4F shows the C-index curve. It is clear from the above results that the risk model has higher predictive accuracy and outperforms other clinical traits such as age, gender, grading, and stage. Nomogram is a predictive tool for quantitatively analyzing clinical outcomes in patients with laryngeal carcinoma. We made nomo plots based on risk scores and other clinical traits (Figure 5A), and calibration plots showed consistency with the prediction results of nomo plots (Figure 5B).

The correlation between ferroptosis-related lncRNA and disease grading and clinical features.

To investigate the clinical effect of ferroptosis-related lncRNA prognostic markers, we compared the differences in clinical case characteristics between high- and low-risk groups, and the results showed that there were statistically

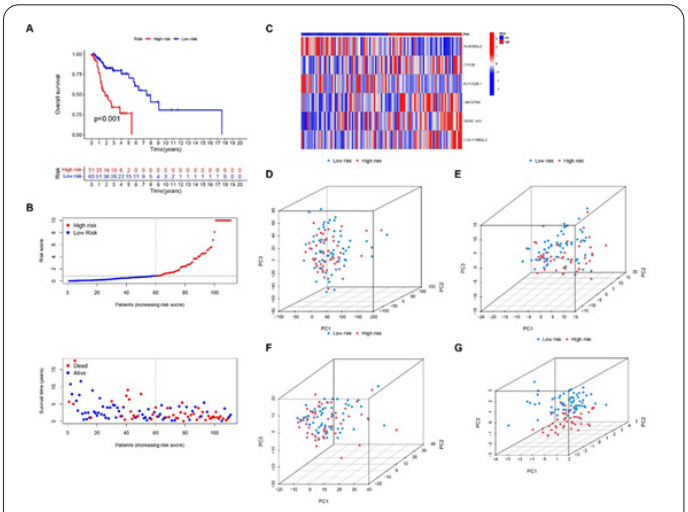

Figure 3. Validation and Principal Component Analysis of Ferroptosis-Related lncRNAs in the Entire Cohort. (A)-(C) Survival status, risk score, and heatmap in the entire cohort. (D) Principal component analysis of all genes in the high and low-risk groups. (E) Principal component analysis of Ferroptosis-Related genes in the high and low-risk groups. (F) Principal component analysis of Ferroptosis-Related lncRNAs in the high and low-risk groups. (G) Principal component analysis of risk-associated lncRNAs in the high and low-risk groups.

Table 1. Ferroptosis-related lncRNA associated with prognosis.

ID	HR	HR.95L	HR.95H	P-value
AC083862.2	0.093562025	0.019242288	0.454927851	0.003324167
AL031186.1	2.036270354	1.060739778	3.908967157	0.032583312
HOXB-AS2	2.912744271	1.141957385	7.429418385	0.025232653
TBILA	2.157709294	1.007657637	4.620328597	0.04774845
LINC02454	4.102839351	1.473504225	11.42398539	0.00689449
AC127526.5	2.728023166	1.377333964	5.403272256	0.004000736
LINC02086	4.341583308	1.063901923	17.71718353	0.04072739
CYTOR	6.208902352	1.360245269	28.34082153	0.018417202
AC010789.1	0.611167416	0.416300295	0.897250411	0.011957339
AC110611.2	5.838546679	1.11496944	30.5735979	0.036726328
KLHL7-DT	6.346998999	1.29711799	31.05684803	0.022543914
AC114296.1	0.331031915	0.110954088	0.98763489	0.047448663
LSAMP-AS1	2.94898008	1.381316935	6.295791569	0.005193532
AP000873.2	10.39198495	1.790685701	60.30837859	0.009071917
KC877982.1	1.334485413	1.055941542	1.686505594	0.015706343
AC012447.1	4.895980936	1.268318807	18.89952998	0.021174022
LINC02768	4.855761987	1.494641058	15.77530896	0.008577099
AP003327.2	0.200660087	0.044497691	0.904866519	0.036613246
AC009268.2	4.839485655	1.111851341	21.06452594	0.035618597
AC104472.4	5.099163399	1.222643389	21.26659957	0.025361577
BX322234.2	0.103356621	0.014354787	0.744183196	0.024239233
GATA2-AS1	2.549798448	1.39506305	4.660342864	0.002350105
AL158166.1	3.062911341	1.427979924	6.569718334	0.004040447
LINC02154	1.663565399	1.165065582	2.375359703	0.005100078
AC004034.1	0.290867407	0.088945548	0.951186994	0.041077428
HM13-IT1	3.293908243	1.270779598	8.537933355	0.014163809
LINC00520	1.669661043	1.017628874	2.739474154	0.042444289
CTB-178M22.2	8.662824976	1.689607474	44.41536731	0.009628823

Table 2. Comparison of General Clinical Characteristics between Two Groups of Patients.

Covariates	Type	Total	Test	Train	P
Age	<=65	73(65.77%)	40(72.73%)	33(58.93%)	0.1829
Age	>65	38(34.23%)	15(27.27%)	23(41.07%)	
Gender	FEMALE	20(18.02%)	11(20%)	9(16.07%)	0.7707
Gender	MALE	91(81.98%)	44(80%)	47(83.93%)	
Grade	G1	8(7.21%)	4(7.27%)	4(7.14%)	0.9875
Grade	G2	70(63.06%)	35(63.64%)	35(62.5%)	
Grade	G3	29(26.13%)	14(25.45%)	15(26.79%)	
Grade	unknown	4(3.6%)	2(3.64%)	2(3.57%)	
Stage	Stage I	2(1.8%)	2(3.64%)	0(0%)	0.5551
Stage	Stage II	9(8.11%)	5(9.09%)	4(7.14%)	
Stage	Stage III	14(12.61%)	7(12.73%)	7(12.5%)	
Stage	Stage IV	71(63.96%)	35(63.64%)	36(64.29%)	
Stage	unknown	15(13.51%)	6(10.91%)	9(16.07%)	
T	T1	7(6.31%)	6(10.91%)	1(1.79%)	0.2733
T	T2	12(10.81%)	6(10.91%)	6(10.71%)	
T	T3	25(22.52%)	11(20%)	14(25%)	
T	T4	54(48.65%)	27(49.09%)	27(48.21%)	
T	unknown	13(11.71%)	5(9.09%)	8(14.29%)	
M	M0	40(36.04%)	20(36.36%)	20(35.71%)	1
M	M1	1(0.9%)	0(0%)	1(1.79%)	
M	unknown	70(63.06%)	35(63.64%)	35(62.5%)	
N	N0	39(35.14%)	21(38.18%)	18(32.14%)	0.4668
N	N1	12(10.81%)	5(9.09%)	7(12.5%)	
N	N2	39(35.14%)	19(34.55%)	20(35.71%)	
N	N3	2(1.8%)	2(3.64%)	0(0%)	
N	unknown	19(17.12%)	8(14.55%)	11(19.64%)	

significant differences in tumor grading and staging in the high-risk group (Figure 5C). We compared the clinical survival time between the high and low-risk groups, in which the survival time was longer in the low-risk group for patients with stage I-II and III-IV, and the difference was statistically significant ($P < 0.05$) (Figure 5D, E).

Pathway enrichment analysis and gene enrichment analysis of ferroptosis-related lncRNA.

To investigate the biological functions and pathway

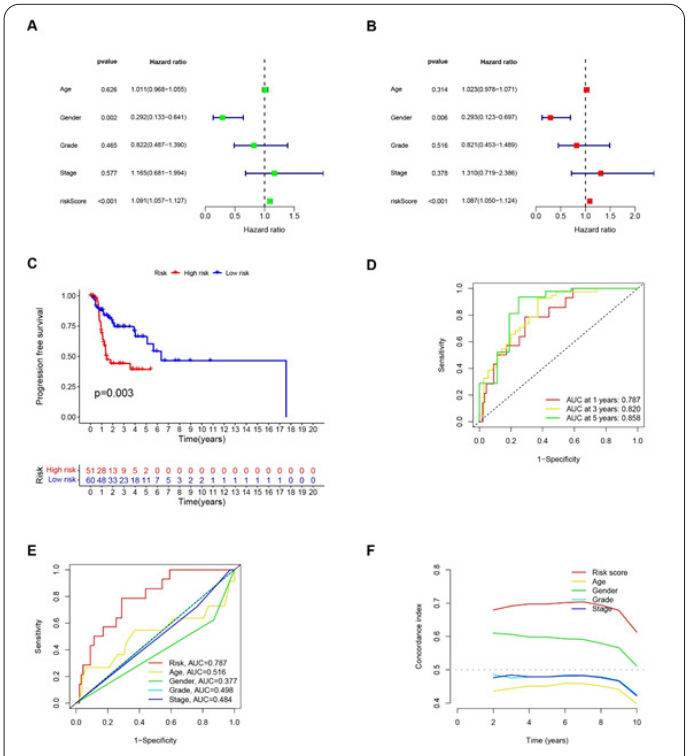

Figure 4. Independence of Ferroptosis-Related lncRNA Prognostic Markers in Predicting Overall Survival Rate. (A) Univariate Cox regression analysis of the predictive model. (B) Multivariate Cox regression analysis of the predictive model. (C) Survival curves of the predictive model in the entire population. (D) AUC values of the predictive model for 1-year, 3-year, and 5-year survival rates. (E) ROC curve of the predictive model for 5-year overall survival. (F) C-index of the predictive model.

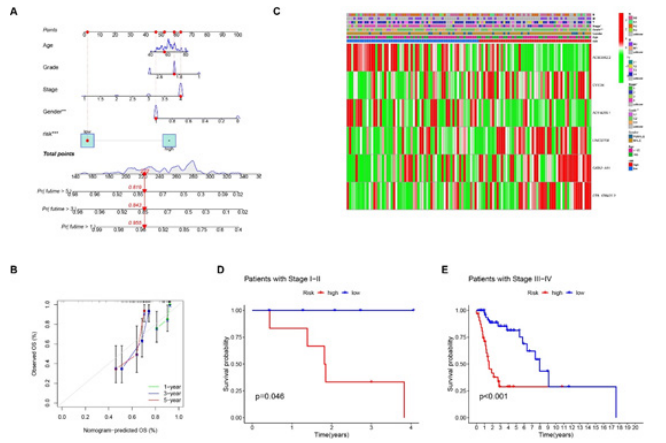

Figure 5. Calibration Plot of Ferroptosis-Related lncRNA and its Association with Disease Grade and Stage. (A) Calibration plot based on all independent predictor variables. (B) Calibration curve of the volcano plot. (C) Relationship between the Ferroptosis-Related lncRNA predictive model and clinical grade and stage. (D), (E) Survival curves of the predictive model in different disease grades.

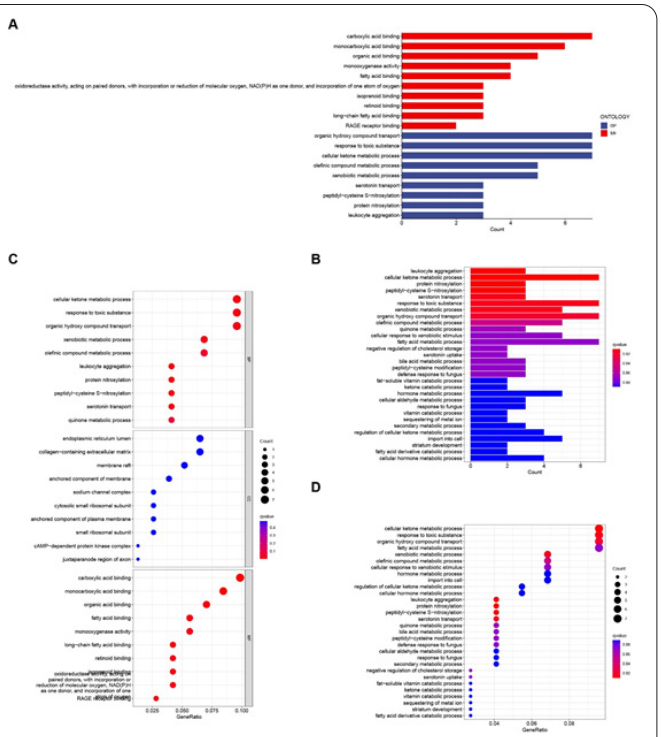

Figure 6. Pathway Enrichment Analysis and Gene Enrichment Analysis of Ferroptosis-Related lncRNA. (A) Bar plot of GO analysis for Ferroptosis-Related lncRNA. (B) Bar plot of KEGG analysis of Ferroptosis-Related lncRNA. (C) Bubble plot of gene enrichment analysis for Ferroptosis-Related lncRNA. (D) Bubble plot of pathway enrichment analysis for Ferroptosis-Related lncRNA.

analysis of differentially expressed genes (DEGs) between high and low-risk groups, we conducted Gene Ontology (GO) and Kyoto Encyclopedia of Genes and Genomes (KEGG) enrichment analyses. In total, we identified 94 DEGs. In the biological process category, these genes were primarily associated with the transport of organic hydroxy compounds, responses to toxic substances, and cellular ketone metabolic processes. In the molecular function category, genes were predominantly involved in carboxylic acid binding, monocarboxylic acid binding, and organic acid binding (Figure 6A, C). KEGG enrichment pathway analysis results indicated associations with leukocyte aggregation, fatty acid metabolic processes, and negative regulation of cholesterol storage (Figure 6B, D).

Construction of co-expression network for ferroptosis-related lncRNA.

The six ferroptosis-related lncRNAs and their associated gene co-expression networks are shown in Figure 7. Among these lncRNAs, AC083862.2 was closely associated with six ferroptosis-related genes (IFNG, PARP12, PARP10, PARP14, PARP9, and TRIM21), and CTB-178M22.2 and AC114296.1 were closely associated with three ferroptosis-related genes. The intrinsic relationship between ferroptosis-related lncRNAs and ferroptosis genes was represented by the Sankey diagram, as shown in Figure 7A and B.

Correlation between ferroptosis-related lncRNAs and immune infiltration.

The heatmap of different immune cell fractions (immune responses) based on six different algorithms is shown in Figure 8A. Some immune cells were associated

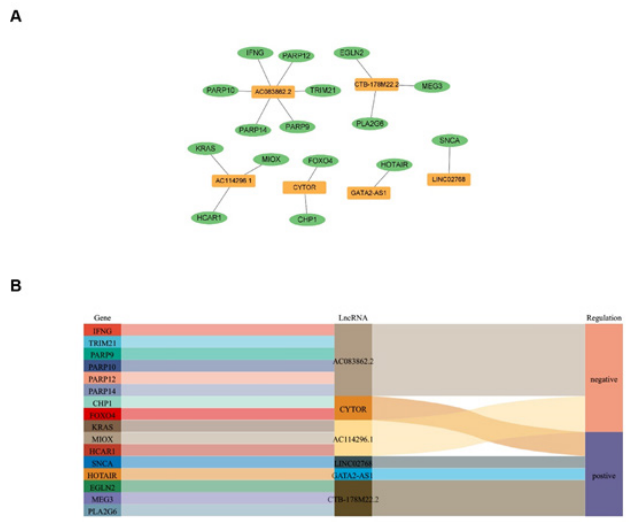

Figure 7. Construction of Co-expression Networks. (A) Co-expression network of 6 Ferroptosis-Related lncRNA and 16 Ferroptosis-Related genes. (B) Sankey diagram network showing the co-expression of 6 Ferroptosis-Related lncRNA and their associated Ferroptosis-Related genes.

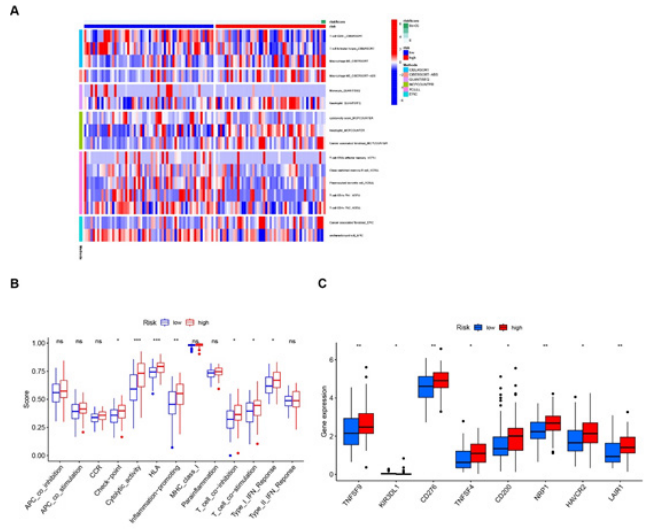

Figure 8. Correlation between Ferroptosis-Related lncRNA and Immune Infiltration. (A) Heatmap showing the correlation between Ferroptosis-Related lncRNA and immune cell infiltration types. (B) Correlation between Ferroptosis-Related lncRNA and immune functions. (C) Expression levels of immune checkpoint genes associated with Ferroptosis-Related lncRNA.

with high risk, including Macrophage M0 of CIBERSORT, Macrophage M0 cells of CIBERSORT-ABS, Neutrophil cells of QUANTISEQ, Neutrophil cells of MCPCOUNTER, Cancer-associated fibroblast cells and Cancer-associated fibroblast cells from EPIC. The immune function ssGSEA score was used to examine the relationship between immune score and immune status. The results showed that immune checkpoints, lysis activity, inflammation promotion, HLA, T-cell co-inhibition, T-cell co-stimulation, and type I IFN response significantly differed in the two groups (Figure 8B). We further investigated the changes in immune checkpoint expression, as shown in Figure 8C, and found that the expression levels of most immune checkpoint molecules were increased in the high-risk group, suggesting that immune checkpoint inhibitors may be potentially effective for treating high-risk patients (Figure 8C).

Correlation between ferroptosis-related lncRNAs and drug sensitivity.

The drug sensitivity analysis of the ferroptosis-related lncRNA risk model was performed using R language, resulting in the identification of 9 drugs that were sensitive to ferroptosis-related lncRNAs. The risk scores and IC50 values for these drugs are shown in Figure 9(A-H).

LncRNA GATA2-AS1 promotes malignant phenotypes in laryngeal squamous carcinoma.

We further evaluated the expression level of LncRNA GATA2-AS1 in laryngeal squamous carcinoma. We achieved knockdown of LncRNA GATA2-AS1 using transient transfection in TU686 and AMC-HN-8 cells, and qRT-PCR confirmed the transfection efficiency (Figure 10A). Next, we assessed its role in regulating laryngeal squamous carcinoma cell proliferation using the Cell Counting Kit-8 (CCK-8) assay and clone formation assay (Figure 10B-C). Knockdown of LncRNA GATA2-AS1 significantly inhibited cell proliferation of TU686 and AMC-HN-8 compared to controls. Then, we used wound healing assays and Transwell assays to verify cell migration and cell invasion (Figure 10D-F). Interestingly, the knockdown of LncRNA GATA2-AS1 significantly inhibited cell migration and cell invasion of TU686 and AMC-HN-8 compared to the control group. The above results imply that lncRNA GATA2-AS1 can promote the proliferation, migration, and invasion of TU686 and AMC-HN-8 cells.

Discussion

Several lncRNAs, including H19, HOTAIR, and ST7-AS1, are associated with the occurrence and development of laryngeal carcinoma (15). In this study, we obtained

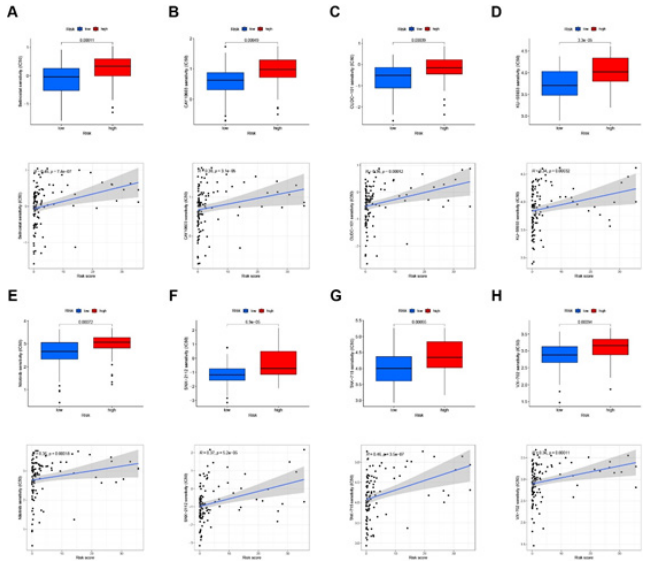

Figure 9. Differential Sensitivity to Different Drugs between Two Groups. (A) Sensitivity difference to belinostat, P=0.00011. (B) Sensitivity difference to CAY10603, P=0.00049. (C) Sensitivity difference to CUDC-101, P=0.00039. (D) Sensitivity difference to KU-55933, P=3.3e-05. (E) Sensitivity difference to Nilotinib, P=0.00072. (F) Sensitivity difference to SNX-2112, P=6.9e-05. (G) Sensitivity difference to TAK-715, P=0.00055. (H) Sensitivity difference to VX-702, P=0.00094.

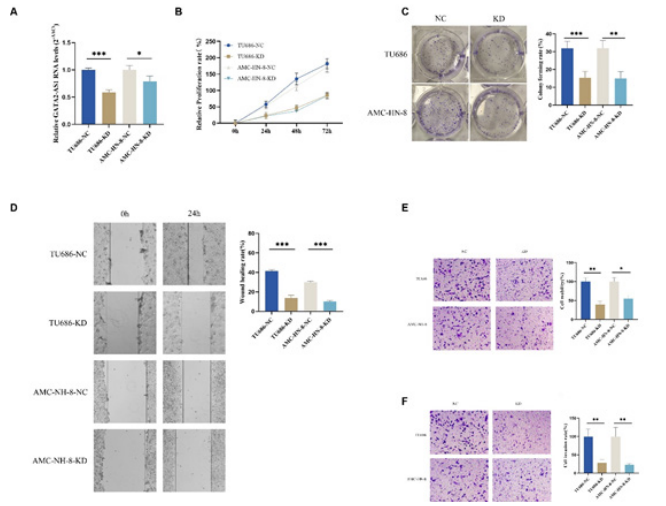

Figure 10. LncRNA GATA2-AS1 promotes malignant phenotypes in laryngeal squamous carcinoma. (A)The knockdown efficiency of lncRNA GATA2-AS1 was verified by qRT-PCR. (B)(C)CCK8 and clonal formation experiments verified the effect of knockdown lncRNA GATA2-AS1 on cell proliferation. (D)The effect of knocking down lncRNA GATA2-AS1 on cell migration was verified by cell scratch experiments. (E) (F) transwell experiment verified the effect of knockdown lncRNA GATA2-AS1 on cell migration and cell invasion.

484 ferroptosis-related genes and 2066 ferroptosis-related lncRNAs.After tumor difference analysis, univariate and multifactorial Cox regression analysis, and Lasso regression analysis, we identified six ferroptosis-related lncRNAs associated with prognosis.They were AC083862.2, CYTOR, AC114296.1, LINC02768, GATA2-AS1, and CTB-178M22.2. Related studies have found that CTYOR is involved in the development of multiple tumors (16). Liu et al. (17) found that lncRNA CYTOR can promote tamoxifen resistance in breast cancer by sponging miR-125a-5p. Zhu et al. (18) found that lncRNA CYTOR can promote aberrant glycolysis and mitochondrial respiration in oral squamous cell carcinoma by interacting with HNRNPC and inhibiting the non-ubiquitinated degradation of HNRNPC, leading to the maintenance of ZEB1 stability. Wang et al. (19) found that lncRNA CYTOR can regulate the BAG3 protein by targeting miR-136-5p interacting with the target gene MAT2B, which can thereby promote proliferation, invasion, and suppress apoptosis in renal cell carcinoma. Pan et al. (20) found that lncRNA GATA2-AS1 stabilizes GATA2 mRNA by recruiting DDX3X and forms a feedback loop with GATA2 to promote proliferation, invasion, epithelial-mesenchymal transition, and stemness in colorectal cancer cells. Man HSJ et al. (21) found that the lncRNA GATA2-AS1 enhances HIF1α induction and regulates hypoxic signaling. However, there are few reports on AC083862.2, AC114296.1, LINC02768, and CTB-178M22.2. The screened lncRNAs are to be explored in further basic scientific research experiments.

With the progress of molecular pathology research, more and more molecular markers have been applied to assess the prognosis of laryngeal carcinoma. However, the prognostic assessment of patients by the influence of a single gene or single clinical factor is limited in accuracy, and patients need more rigorous prognostic models to assess and guide precise treatment (22). In this paper, we validated the accuracy of our constructed risk model by R. We classified patients into high- and low-risk groups using the Kaplan-Meier method. We visually predicted the degree of differentiation between the high- and low-risk groups using principal component analysis (PCA), and the results indicated that patients were effectively divided into two clusters, indicating the validity of the grouping. Next, we used ROC curves to predict the accuracy of ferroptosis-related lncRNA biomarkers in patient survival at 1, 3, and 5 years, and the results showed that the prognostic model constructed based on ferroptosis-related lncRNA showed good prognostic efficacy in the patient data (all AUC > 0.07). Combining clinical information with information related to prognostic biomarkers, we established a nomogram to predict the prognosis of laryngeal carcinoma, and the calibration plots were consistent with the nomogram prediction results. The above indicates that ferroptosis-related lncRNA prognostic markers are independent in predicting the overall survival of patients. In this article, we investigated the clinical role of ferroptosis-related lncRNA prognostic markers. We found that the risk coefficient distribution was statistically different in clinical stage I-II and clinical stage III-IV, indicating that the prediction model is feasible for clinical practice.

We constructed co-expression networks and Sankey diagrams to investigate the genetic linkage of ferroptosis-associated lncRNAs. An immune infiltration analysis of ferroptosis-related lncRNAs was performed. The results revealed statistically significant differences in immune cell comparisons between high and low-risk groups ($P < 0.05$), and the high-risk cohort had higher immune infiltration scores and immune checkpoint scores. Relevant evidence suggests that ferroptosis is synergistically enhanced by combined antitumor therapy with immune checkpoints (23). Therefore, these lncRNAs associated with ferroptosis may be targets for combination immune checkpoint inhibitor therapy. Wang et al. first reported that CD8+ T cells decreased SLC7A11 and SLC3A2 expression and increased iron-specific lipid peroxidation in cancer cells by releasing interferon γ (IFNγ) (24). In our study, the high-risk group had higher expression of ICIs. For example, CD276 expression was significantly higher in the high-risk group, increasing the likelihood that these patients would benefit from anti-CD276 immunotherapy, which is a unique immune target for HNSCC in head and neck tumors (25,26). According to the results of pharmacoresensitivity studies, high-risk patients are more sensitive to drugs such as belinostat.

We performed functional enrichment analysis to investigate the potential biological mechanisms of ferroptosis-associated lncRNAs. GO, and KEGG results showed that differentially expressed lncRNAs were mainly clustered in leukocyte aggregation, fatty acid metabolic processes, and negative regulation of cholesterol storage. This suggests that ferroptosis-associated lncRNAs may influence laryngeal carcinoma progression in these aspects.

GATA2-AS1 (GATA2 Antisense RNA 1) is a long non-coding RNA found to function in colorectal cancer and hypoxia. We validated the role of GATA2-AS1 on cell phenotype in TU686 and AMC-HN-8 cell lines. We found that GATA2-AS1 was expressed at increased levels in laryngeal carcinoma and could promote cell proliferation, migration, and invasion or be a potential therapeutic target for laryngeal carcinoma.

Although this paper presents a prognostic model of ferroptosis-related lncRNA associated with laryngeal carci-

noma prognosis, the study still has some limitations. First, the data in this paper were obtained from the TCGA database, and a patient cohort needed to be included for data validation. Second, additional functional validation experiments on the remaining critical lncRNAs in this model are needed to reveal the specific mechanisms of ferroptosis lncRNAs in laryngeal carcinoma progression. The above clinical study limitations are expected to be further investigated.

In conclusion, a prognostic model of laryngeal carcinoma based on ferroptosis-related lncRNA was constructed in this paper, which can predict the prognosis of laryngeal carcinoma and can guide the clinical diagnosis and treatment of laryngeal carcinoma. However, the research progress and molecular mechanism of ferroptosis-related lncRNA in laryngeal carcinoma still need further study.

Acknowledgment
The study was supported by the Major Science and Technology Plan Project of Hainan Province (ZDKJ202005), Science and Technology Plan Project of Hainan Province (LCYX202105, LCYX202202) and supported by Hainan Province Clinical Medical Center.

Conflict of Interests
The authors declared no conflict of interest.

References

1. Karatzanis AD, Psychogios G, Waldfahrer F, et al. Management of locally advanced laryngeal cancer. J Otolaryngol-Head N 2014; 43(1): 4.
2. Steuer CE, El-Deiry M, Parks JR, Higgins KA, Saba NF. An update on larynx cancer. Ca-Cancer J Clin 2017; 67(1): 31-50.
3. Tang D, Kang R, Berghe TV, Vandenabeele P, Kroemer G. The molecular machinery of regulated cell death. Cell Res 2019; 29(5): 347-364.
4. Stockwell BR, Friedmann AJ, Bayir H, et al. Ferroptosis: A Regulated Cell Death Nexus Linking Metabolism, Redox Biology, and Disease. Cell 2017; 171(2): 273-285.
5. Xie Y, Hou W, Song X, et al. Ferroptosis: process and function. Cell Death Differ 2016; 23(3): 369-379.
6. Gao N, Li Y, Li J, et al. Long Non-Coding RNAs: The Regulatory Mechanisms, Research Strategies, and Future Directions in Cancers. Front Oncol 2020; 10: 598817.
7. Statello L, Guo CJ, Chen LL, Huarte M. Gene regulation by long non-coding RNAs and its biological functions. Nat Rev Mol Cell Bio 2021; 22(2): 96-118.
8. Ai W, Li F, Yu HH, Liang ZH, Zhao HP. Up-regulation of long noncoding RNA LINC00858 is associated with poor prognosis in gastric cancer. J Gene Med 2020; 22(7): e3179.
9. Gai C, Liu C, Wu X, et al. MT1DP loaded by folate-modified liposomes sensitizes erastin-induced ferroptosis via regulating miR-365a-3p/NRF2 axis in non-small cell lung cancer cells. Cell Death Dis 2020; 11(9): 751.
10. Jiang W, Song Y, Zhong Z, Gao J, Meng X. Ferroptosis-Related Long Non-Coding RNA Signature Contributes to the Prediction of Prognosis Outcomes in Head and Neck Squamous Cell Carcinomas. Front Genet 2021; 12: 785839.
11. Zhou N, Bao J. FerrDb: a manually curated resource for regulators and markers of ferroptosis and ferroptosis-disease associations. Database-Oxford 2020; 2020: baaa021.
12. Li T, Fu J, Zeng Z, et al. TIMER2.0 for analysis of tumor-infiltrating immune cells. Nucleic Acids Res 2020; 48(W1): W509-W514.
13. Yi M, Nissley DV, McCormick F, Stephens RM. ssGSEA score-based Ras dependency indexes derived from gene expression data reveal potential Ras addiction mechanisms with possible clinical implications. Sci Rep-Uk 2020; 10(1): 10258.
14. Topalian SL, Taube JM, Anders RA, Pardoll DM. Mechanism-driven biomarkers to guide immune checkpoint blockade in cancer therapy. Nat Rev Cancer 2016; 16(5): 275-287.
15. Falco M, Tammaro C, Takeuchi T, et al. Overview on Molecular Biomarkers for Laryngeal Cancer: Looking for New Answers to an Old Problem. Cancers 2022; 14(7): 1716.
16. Liang J, Wei X, Liu Z, et al. Long noncoding RNA CYTOR in cancer: A TCGA data review. Clin Chim Acta 2018; 483: 227-233.
17. Liu Y, Li M, Yu H, Piao H. lncRNA CYTOR promotes tamoxifen resistance in breast cancer cells via sponging miR-125a-5p. Int J Mol Med 2020; 45(2): 497-509.
18. Zhu W, Wang J, Liu X, et al. lncRNA CYTOR promotes aberrant glycolysis and mitochondrial respiration via HNRNPC-mediated ZEB1 stabilization in oral squamous cell carcinoma. Cell Death Dis 2022; 13(8): 703.
19. Wang D, Zhu X, Siqin B, Ren C, Yi F. Long non-coding RNA CYTOR modulates cancer progression through miR-136-5p/MAT2B axis in renal cell carcinoma. Toxicol Appl Pharm 2022; 447: 116067.
20. Pan Y, Zhu Y, Zhang J, Jin L, Cao P. A feedback loop between GATA2-AS1 and GATA2 promotes colorectal cancer cell proliferation, invasion, epithelial-mesenchymal transition and stemness via recruiting DDX3X. J Transl Med 2022; 20(1): 287.
21. Man H, Subramaniam N, Downs T, et al. Long noncoding RNA GATA2-AS1 augments endothelial hypoxia inducible factor 1-alpha induction and regulates hypoxic signaling. J Biol Chem 2023; 299(5): 103029.
22. Hamilton DW, O'Hara J, Rajgor A, et al. Precision medicine in laryngeal cancer: protocol of the laryngeal cancer cohort (LARCH). Bmj Open 2023; 13(1): e67561.
23. Deng J, Zhou M, Liao T, et al. Targeting Cancer Cell Ferroptosis to Reverse Immune Checkpoint Inhibitor Therapy Resistance. Front Cell Dev Biol 2022; 10: 818453.
24. Wang W, Green M, Choi JE, et al. CD8(+) T cells regulate tumour ferroptosis during cancer immunotherapy. Nature 2019; 569(7755): 270-274.
25. Alsaedy H, Mirzaei A, Alhashimi RA. Investigating the structure and function of Long Non-Coding RNA (LncRNA) and its role in cancer. Cell Mol Biomed Rep 2022;2(4), pp. 245-253. doi: 10.55705/cmbr.2022.360799.1062
26. Wang C, Li Y, Jia L, et al. CD276 expression enables squamous cell carcinoma stem cells to evade immune surveillance. Cell Stem Cell 2021; 28(9): 1597-1613.